Triggered Ion-acoustic Waves

By Forrest Mozer[1], Stuart Bale[1], Paul.Kellogg[3], Roberto Livi[2], Orlando Romeo[2], Ivan Vasko[2], and Jaye Verniero[4]

1. Physics Department and Space Sciences Laboratory, University of California, Berkeley,94720
2. Space Sciences Laboratory, University of California, Berkeley,94720
3. University of Minnesota, Minneapolis, Minnesota, 55455
4. Goddard Space Flight Center, Greenbelt,Md., 20706

Corresponding author: Forrest.Mozer@gmail.com

The Parker Solar Probe is in a solar orbit with a perihelion for orbit 12 at 13.3 solar radii. The electric field experiment on this satellite observes what we call triggered ion-acoustic waves as the most dominant wave mode above a few Hz within the solar radial distance of 15-25 solar radii. In this mode, a few Hz electrostatic wave is typically accompanied by bursts of a few hundred Hz wave whose bursts are phase locked with each low frequency wave period. Plasma density fluctuations with $\Delta n/n \sim 0.1$ accompany these waves and they have no magnetic field component. The wave durations can be hours and their field and density fluctuations are nearly pure sine waves. They are identified as ion-acoustic waves. The low and high frequency waves are measured to have the same phase velocity within experimental uncertainties, which is a requirement associated with their phase locked relationship. From the measured wavelength, the potential associated with the low frequency wave is estimated to be ~10 Volts, which can result in electron heating via the Landau resonance that is in agreement with observations of the core electron temperature increases at times of such waves. Their phase locked relationship and pure frequency are surprising features that characterize a new regime of instability and evolution of ion-acoustic waves that may not have been reported previously. That these waves are an instrumental effect unrelated to natural processes is considered. While this is unlikely, the possibility that these waves are artificial cannot be rule out.

OVERVIEW

This paper reports the surprising observation of coupled and phase locked electrostatic waves that move together even though their frequencies differ by a factor of more than 100, that exist for hours at a time, and whose spectra are pure sine waves. Because these amazing results are not understood theoretically, it is important to consider the possibility that they are artifacts unrelated to processes occurring in the natural plasma. To include this possibility, the main body of the paper discusses these triggered ion-acoustic waves as real phenomena and the appendix considers whether they are real or artificial. The conclusion is that the triggered ion-acoustic waves are likely to be natural signals in the plasma although an instrumental effect cannot be excluded.

I INTRODUCTION

The Parker Solar Probe has measured triggered ion-acoustic waves in each of the seven orbits that passed through the altitude range of 15-25 solar radii. Triggered ion-acoustic waves have the following properties:

- A pair of coupled waves, one of which is at a frequency of a few Hertz and the other is at few hundred Hertz
- These waves are electrostatic ion-acoustic waves because they do not have magnetic components, they contain important density fluctuations, and their phase speeds are the order of the ion-acoustic speed [Mozer et al, 2021].
- The two waves are coupled such that the high frequency wave sometimes occurs in short bursts during successive periods of the low frequency wave and at a fixed phase of this lower frequency wave.
- Both waves are narrow band, effectively pure sine waves. (Normal ion-acoustic waves are broadband [Kurth et al., 1979; Mozer et al., 2020]).
- They can exist as a pair for times as long as several hours. (Normal ion-acoustic waves have much shorter durations [Kurth et al., 1979; Mozer et al., 2020]).
- They are associated with heating the core electron distribution [Mozer et al, 2022a] so they may be significant for solar wind dynamics.

The Parker Solar Probe is in a solar orbit with one surface (the heat shield) facing the Sun near perihelion. The line of sight from the spacecraft to the Sun is the spacecraft Z-direction, along which the typical magnetic field and solar wind flow are oriented near perihelion. The X-Y plane, perpendicular to the Sun-satellite line, contains a two-component electric field and spacecraft potential measurement by antennas that are not much larger than the spacecraft [Bale et al, 2016]. By fitting the measured spacecraft potential to the low rate density measurements obtained from the SWEAP plasma measurements [Kasper et al, 2016; Whittlesey et al, 2019], higher frequency estimates of the plasma density and density fluctuations [Mozer et al, 2022b] are obtained. In addition, the SWEAP instrument provided the solar wind velocity and ion beam data utilized in the following analyses. The solar wind speed, magnetic field, plasma density and ion temperature for the events that follow are given in the Appendix.

II EXAMPLE OF TRIGGERED ION-ACOUSTIC WAVES

Figure 1 presents triggered ion-acoustic waves observed on January 19, 2021. The four pairs of panels each display EX and the density fluctuations, $\Delta N/N$. Panel (a), gives 1 Hz high pass filtered electric field data that illustrates the low and high frequency waves that are phase locked such that the high frequency bursts occur at fixed phases of the low frequency signal. Panel (b) illustrates the density fluctuations measured above 1 Hz and they show mainly the low frequency wave signal. Panels (c) and (d) show the low frequency (0.5-2 Hz) components of the triggered ion-acoustic wave with $\Delta E \sim 0.5$ mV/m and $\Delta N/N \sim 0.13$, while pair (e) and (f) illustrate the high frequency (>100 Hz) components having $\Delta E \sim 4$ mV/m and $\Delta N/N \sim 0.004$. Panels (g) and (h) present a short portion of the high frequency component to illustrate that they are nearly pure sine waves, which is not expected or understood for ion-acoustic waves (the full spectral width at half-maximum is less than 60 Hz). The quality of these curves suggest that instrument noise is not a matter of concern for this data set. Figure 1 presents the same event as that described in Figure 6 of Mozer et al [2021a] and it was selected to benefit from this earlier information that shows the phase locking of the low and high frequency waves and the absence of a magnetic field signature during such events. For a 100 km/sec phase velocity of these waves [Mozer et al, 2021], the magnetic field, B, associated with a phase speed E/B~100 km/sec in the presence of a ~1 mV/m low frequency electric field in an electromagnetic wave would be ~10 nT. The upper limit to the

observed magnetic field at the wave frequency is at least an order of magnitude less, showing that these are electrostatic ion-acoustic waves. It is important to note that the potentials of antennas 1 through 4 produce both the electric field and the density data because the difference between potential pairs is the electric field and the sum of the four potentials is the spacecraft potential that gives the plasma density [Mozer et al, 2022b] . Thus, although the origins of the electric field and density are related, they are really two different quantities.

The sine waves in panels (g) and (h) are shifted with respect to each other by 90 degrees. This phase shift is consistent with Ohm's law, according to which the parallel electric field in an ion-acoustic wave is predominantly due to the electron pressure gradient, $eE_{||} = -\nabla_{||} p_e/n$ [e.g., Davidson, 1972; Kelley and Mozer, 1972]. This figure illustrates the phase locked relationship between a few Hz and a few hundred Hz electrostatic wave whose components are nearly pure sine waves. Neither of these properties of ion-acoustic waves have been observed before, to our knowledge. Another significant and previously unobserved property of triggered ion-acoustic waves is that they can exist for times as long as hours or even a day. An example of this fact is given in Figure 4 of Mozer et al [2021].

Figure 2 provides detailed information on the event of Figure 1 that enables an understanding of the geometry in the X-Y plane. As seen in panel 2A, the 600 Hz electric field oscillated in the ±X direction while the component of the solar wind velocity in the X-Y plane was in the –X direction (panel 2C) and the magnetic field in the X-Y plane was inclined about 30^o degrees away from the +X-axis (panel 2B). The direction of wave propagation may be determined from the timing of the signals on each of the antennas. Panel 2D shows that antennas V1 and V4 received the maximum wave signal at about the same time. From the geometry illustrated in Figure 3, this requires that the wave traveled in either the +X or –X direction. If it traveled in the –X direction, the signals on V1 and V4 would precede the signals on V2 and V3, as actually happened in panel 2D. (The negatives of the signals on V2 and V3 are plotted to compensate for the fact that the peak of a wave traveling to the left produces negative voltages on V2 and V3 because they measure the voltage on the antenna minus the voltage of the spacecraft body). In summary, in the spacecraft X-Y plane, the wave propagated in the –X direction of the solar wind flow, the electric field oscillations were along this velocity direction, and the wave propagated in the X-Y plane at an angle of about 30^o with respect to the magnetic field in the X-Y plane. Note that without electric field measurements along the Z-axis, the full wave vector cannot be determined and we have only information about the wave propagation in the XY plane. While, in principle, the timing between the peak signals on V1/V4 and V2/V3 can give the phase velocity of the wave, this is not possible in practice because potential contours around the spacecraft are distorted by the equipotential conducting spacecraft and the conducting short dipole antennas. Instead, the phase velocity and wavelength of the ~1 Hz and 600 Hz waves will be determined from the arguments in Section IV.

III OTHER EXAMPLES OF TRIGGERED ION-ACOUSTIC WAVES

Figure 4 presents another example of triggered ion-acoustic waves observed on November 22, 2021. The three sets of three panels each in this Figure present data that is high pass filtered at 0.5 Hz (panels 4A, 4B, and 4C), bandpass filtered at 0.5-10 Hz (panels 4D, 4E, and 4F), and high pass filtered at greater than 100 Hz (panels 4G, 4H, and 4I). Panels 4A, 4B, 4D, 4E, 4G, and 4H give the two electric field components at the three frequency ranges and panels 4C, 4F, and 4I give the

density fluctuations, ΔN/N. An interesting feature exhibited in panels 4A and 4B is that the higher frequency wave appeared continuously and not just in bursts during a specific phase of the lower frequency waveform as in Figure 1, although the most intense ~60 mV/m high frequency signals were observed at a specific phase of the low-frequency wave. Again, the density fluctuations were shifted by 90 degrees with respect to the electric fields in accordance with the Ohm's law for ion-acoustic waves. In addition, as seen in panels 4G, 4H, and 4I, the field and density fluctuations were almost pure sine waves. The phase locking of the low and high frequency wave is illustrated by the fact that the peak values of the high frequency EX (panel 4A) occurred in phase with the low frequency EX of panel 4D

Figure 5 illustrates the existence of narrow band (panels 5A and 5B), pure sinusoidal (panels 5C and 5D) waves that existed in the absence of a lower frequency component for the 14 minute interval of the event. The spike near the center of the plot is due to a dust impact. This event demonstrates that narrowband electrostatic waves at a few hundred Hz can be observed without a low-frequency counterpart as in Figure 1. Although these waves are not referred to as triggered ion-acoustic waves, we point out in the next section that existing theories have difficulties explaining these narrow band observations.

IV DISCUSSION

Although various ion-acoustic waves are observed on PSP, the most distinct types in the near Sun solar wind are triggered ion-acoustic waves, which are high-frequency ion-acoustic waves phase-locked with low-frequency waves (Figures 1, 2, 4, and 5). In this section, we provide estimates of the speed, wavelength and amplitude of the electrostatic potential of such triggered ion-acoustic waves.

Their phase-locked behavior implies that the high- and low-frequency ion-acoustic waves propagate in the same direction and have identical phase speeds in any frame, so

$$phase\ speed = 2\pi f_h/k_h = 2\pi f_l/k_l \quad \text{or} \quad f_h/f_l = k_h/k_l \tag{1}$$

where k_h and k_l are wave numbers of high- and low-frequency waves, and f_h and f_l are their frequencies. For triggered ion-acoustic waves in Figure 1, $k_h/k_l \approx 460$ since, in the spacecraft frame, $f_h \approx 600$ Hz and $f_l \approx 1.3$ Hz.

This ratio of the wavenumbers of the low- and high-frequency waves can be estimated by an alternative method based on Ohm's law [Kelley and Mozer, 1972]. Since the observed waves are expected to have phase speeds much smaller than the electron thermal speed, the parallel electric field should be balanced by the electron pressure gradient

$$enE_{||} = -\nabla_{||} p_e \tag{2}$$

For planar electrostatic waves Eq. (2), may be written along the wave vector and an estimate of the wavenumber is

$$k \approx \frac{e\,E}{T_e(\delta n/n)} \tag{3}$$

where k is the full wavenumber and not a component, E is the total amplitude of electric field fluctuations, T_e is the electron temperature, and $\delta n/n$ is the amplitude of density fluctuations. Importantly, PSP measures only the electric field in the XY plane, while the wave vector can be oblique to that plane. To take this into account, Eq. (3) is written as follows

$$k \approx \frac{e\,E_{XY} / \cos\theta_{kXY}}{T_e\,(\delta n/n)} \tag{4}$$

where E_{XY} is the measured electric field amplitude in the XY plane and θ_{kXY} is the angle between the wave vector and the XY plane. Since the phase-locking condition implies the propagation direction of low- and high-frequency waves are identical, Eq. (4) allows obtaining the relation between wavenumbers of the high- and low-frequency waves as

$$\frac{k_h}{k_l} \approx \frac{[E_{XY}/\delta n]_h}{[E_{XY}/\delta n]_l} \tag{5}$$

The critical question is whether the ratio of the wavenumbers predicted by Eq. (5) is consistent with that predicted by the phase-locking condition given by Eq. (1). For the 600 Hz waves of Figure 1, the electric field amplitude was 4 mV/ and $\delta n/n$ was 0.004, while for the ~1.3 Hz waves in the same interval the electric field was 0.5 mV/m and $\delta n/n$ was 0.13. Using these values in Eq. (5) gives $k_h/k_l \approx 260$, which is about a factor of two smaller than the estimate obtained using Eq. (1). These two estimates are equal within the uncertainties of the frequency response factors of the antennas and the uncertainties associated with estimates of density fluctuations based on measurements of spacecraft potential [Mozer et al, 2022b]. The rough consistency between k_h/k_l given by the equivalence of Eq. (1) and Eq. (5) indicates that triggered ion-acoustic waves correspond to a physical process, rather than being an instrumental effect. Another indication that triggered ion-acoustic waves are a real phenomenon is that the electric field and density fluctuations were shifted with respect to each other by 90 degrees, in accordance with Ohm's law, as has been discussed.

We can estimate the amplitude δφ of the electrostatic potential of both waves without knowledge of the angle θ_{kXY}. Taking into account that according to Eq. (2), $e\delta\varphi/T_e \approx \delta n/n$ and that the local electron temperature for the interval in Figure 1 was about 54 eV, we find that

$$\delta\varphi_h \approx 0.2\,V \quad \text{and} \quad \delta\varphi_l \approx 7\ \text{V} \tag{6}$$

Since ion-acoustic waves have speeds much slower than the electron thermal speed, the electron heating due to their interaction with these waves via the Landau resonance can only be less than or the order of their potentials. Thus, the direct electron heating due to the high-frequency waves cannot exceed 1%, while the direct heating due to the low-frequency waves can be as large as 10%. This amount of heating is consistent with the core electron temperature increases that have been observed at the times of these waves [Mozer et al, 2021a]. Also, note that because this is an active

plasma, the electrons can acquire additional heat by transfer of energy from the ions to electrons via the triggered ion acoustic waves whose amplitude may not affect this transfer rate.

According to Eqs. (1) and (4) the wavelength of the low- and high-frequency waves may be estimated as follows

$$\lambda_h \approx 2\pi(T_e/eE_{XY})(\delta n/n)\cdot\cos\theta_{kXY} \approx 340\ m\cdot\cos\theta_{kXY} \text{ and } \quad \lambda_l \approx 460\ \lambda_h \tag{7}$$

The value of θ_{kXY} is not known, since ion-acoustic waves can propagate at an arbitrary angle with respect to the local magnetic field, as shown, for example, in theory [Gary and Omidi, 1987] and observations in the Earth's bow shock [Hull et al., 2006; Vasko et al., 2022]. However, reasonable assumptions on the propagation direction and values of the plasma frame speed V_0, of the observed waves allow estimating reasonable ranges of θ_{kXY} values. First, Figure 6 shows that the ion distribution functions associated with the triggered ion-acoustic waves of Figure 1 consisted of a beam population streaming at about 200 km/s anti-sunward. (The beam flux is a maximum at ~150 km/sec and is down by two orders-of-magnitude by 300 km/sec, so a typical value for the beam speed of 200 km/sec seems reasonable). The presence of an ion beam indicates that it is the likely source of a linear instability resulting in growth of the ion-acoustic waves, whose further nonlinear dynamics transforms them into the observed triggered ion-acoustic waves. This, in turn, implies that, in the plasma frame, the triggered ion-acoustic waves propagate in the same direction as the beam, such that $\cos\theta_{kV} > 0$, where θ_{kV} is the angle between the wave propagation direction in the plasma frame and solar wind speed. Second, it is reasonable to assume that the plasma frame speed V_0 of the waves is the order of the ion-acoustic speed, ~100 km/s or, more broadly, it might be from a few tens of km/s to about 200 km/s, which is the speed of the beam.

Using the assumptions that $\cos\theta_{kV} > 0$ and V_0 is the order of 100 km/s, we can estimate θ_{kXY} using the observed spacecraft frame frequencies of the waves. The spacecraft frame frequency is related to the plasma frame speed V_0 and angle θ_{kV} as follows

$$2\pi f_h = k_h\,(V_0 + V_{sw}\cos\theta_{kV}) \tag{8}$$

Since the plasma flow velocity is predominantly along –Z (Figure 2) $\cos\theta_{kV} \approx \sin\theta_{kXY}$, where we recall that $0^o \le \theta_{kXY} \le 90^o$ is the angle between the wave vector and the XY plane. Noting that $V_{sw} \approx 200$ km/s and using the wavelength estimate from Eq. (7) we obtain the following relation for θ_{kXY}

$$\cos\theta_{kXY} \approx (V_0/V_{sw} + \sin\theta_{kXY}), \tag{9}$$

where we took into account that $(f_h/V_{sw})\cdot 2\pi(T_e/eE_{XY})(\delta n/n) \approx 1$. Now, taking into account that V_0/V_{sw} is from about 0 to 1 we find θ_{kXY} is in the range from 0^o to 45^o. First, this implies that the triggered ion-acoustic waves propagated obliquely to the local magnetic field at an angle between 45^o and 90^o (note that this is the angle between the full k-vector and the total magnetic field) . Second, along with Eq. (6) this allows estimating the range of wavelengths of the triggered ion-acoustic waves as

$$\lambda_h \approx 240 - 340\ m, \qquad \lambda_l \approx 100 - 150 \text{ km}$$

The Debye length during these measurements was 0.8 meters, so the wavelength of the 600 Hz ion-acoustic wave was about 350 Debye lengths. This is consistent with the phase-locking condition of two ion-acoustic waves, which can be realized due to their negligible dispersion at wavelengths much larger than the Debye length.

An unusual feature of the triggered ion-acoustic waves as well as the non-triggered ion-acoustic wave presented in Figure 7 is that they are narrow band on time scales of minutes and even hours, which is extremely atypical of ion-acoustic waves previously reported in space plasmas. For example, previous observations in the solar wind [Kurth et al., 1979] and the Earth's bow shock [Hull et al., 2006; Vasko et al., 2022] showed that ion-acoustic waves typically have spectral widths comparable with the wave central frequency.

There is a theoretical difficulty explaining narrow band ion-acoustic waves, since these waves are essentially non-dispersive acoustic waves and, even if being produced monochromatically, they are expected to steepen due to fluid nonlinearities [e.g., Davidson, 1972]. The steepening time scale can be estimated as $\lambda/2\pi\ \delta u$, where $\delta u \sim eE/2\pi f_h\ m_i$ is the amplitude of the ion bulk velocity fluctuations due to the electrostatic wave, and f_h is the wave's frequency in the plasma rest frame. Using the observed amplitudes and assuming reasonable phase speeds of 10-200 km/sec for the ion-acoustic waves in the plasma frame, the steepening time scale of both low- and high-frequency waves is a few seconds. Another nonlinear mechanism, which widens the spectral width of an initially monochromatic ion-acoustic wave, is ion trapping by the electrostatic wave [e.g. Davidson, 1972] and this process operates on a time scale of $\lambda/\ 2\pi\delta u$ where $\delta u \sim (e\delta\varphi/m_i)^{1/2}$ is the speed of the trapped ions, which is a few seconds as well. Thus, observations of narrow band ion-acoustic waves on a time scale of minutes and hours implies that nonlinear effects, such as steepening and particle trapping, are somehow prevented or balanced by other mechanisms. This is a theoretical difficulty with explaining observations of narrow band ion-acoustic waves, be they triggered or not.

The mechanism resulting in phase-locking between the high- and low-frequency electrostatic waves remains unknown. Previous observations demonstrated that phase correlation between electrostatic spikes and whistler waves can occur due to the steepening process of the whistler wave electrostatic component under the resonance condition between electron-acoustic and whistler waves [Agapitov et al., 2018; Vasko et al., 2018; An et al., 2019]. This process cannot explain the observed triggered ion-acoustic waves, since the steepening of the low-frequency electrostatic waves would produce electrostatic fluctuations over the broad range of frequencies, rather than narrow band waves at a single frequency. In our analysis, we assumed that the observed phase-locking implies that the high- and low-frequency waves have identical velocities and found that this assumption does not lead to any contradiction, i.e. the ratio of wavenumbers given by Eq. (1) and Eq. (5) are consistent within a factor of two. One can argue however for another scenario potentially explaining the observed phase-locking. Recent simulations showed that electrostatic fluctuations can be observed at a specific phase of an oblique whistler wave, since the drift between cold and hot electrons associated with the whistler wave results in a high-frequency electrostatic instability [Roytershteyn and Delzanno, 2021]. Following this idea one may hypothesize that the phase-locking observed in triggered ion-acoustic waves is due to a current-driven instability producing high-frequency electrostatic waves at the specific phase of the low-frequency

electrostatic wave. In this case, the high frequency waves do not even need to propagate at the same speed and in the same direction as the low-frequency wave; the phase-locking is observed because the high-frequency waves are at the phase where the plasma is unstable. The viability of this mechanism for triggered ion-acoustic waves deserves a separate study, while here we only point out that the ion-electron drift velocity associated with the low-frequency waves is negligible compared to the ion-acoustic speed and, thus, not likely to be unstable.

In summary, the many forms of the structures that we call triggered ion-acoustic waves are not understood. A theory of the generation of a low frequency electrostatic wave in the solar radial range of our observations may provide the first clue about the eventual mechanism [Kellogg, 2022]. Perhaps, additional factors, such as the presence of a dusty plasma, can resolve this difficulty. Such effects have not been investigated.

V ACKNOWLEDGEMENTS

This work was supported by NASA contracts NNN06AA01C and 80NSSC21K0581. The authors acknowledge the extraordinary contributions of the Parker Solar Probe spacecraft engineering team at the Applied Physics Laboratory at Johns Hopkins University. The FIELDS experiment on the Parker Solar Probe was designed and developed under NASA contract NNN06AA01C. Our sincere thanks to P. Harvey, K. Goetz, and M. Pulupa for managing the spacecraft commanding, data processing, and data analysis, which has become a heavy load thanks to the complexity of the instruments and the orbit. We also acknowledge the SWEAP team for providing plasma data. The work of I.V. was supported by National Science Foundation grant No. 2026680.

APPENDIX

In this appendix, eight investigations are described relative to the question of whether the observed triggered ion-acoustic waves are real or artifical.

1. Triggered ion-acoustic waves are observed only between about 15 and 25 solar radii [Mozer et al, 2021]. In this region, there are no whistlers [Cattell et al, 2022] and the triggered waves are by far the most prominent waves above a few Hz in this region. That they are confined to a narrow spatial region may be evidence that they are real because, if they are artifical, it might be supposed that they should appear at any solar radius.

2. Triggered ion-acoustic waves are seen on practically every orbit where they have been searched for. Mozer et al [2021] showed this to be true for orbits 6, 7, 8, and 9, and more recent observations on orbits 10, 11, and 12 also confirm their presence. Their omnipresence in the given radial region may be considered as evidence of their reality.

3. Core electron heating has always been observed in conjunction with triggered ion-acoustic waves [Mozer et al, 2021a] and heating is absent when there are no triggered waves [see Figure 1 of Mozer et al, 2021a] It may be difficult to argue that such waves are artificial

in the face of this correlation of waves with a fundamental property of the evolving solar wind.

4. The triggered ion-acoustic waves also appear when the ratio of the core electron to ion temperature, Te/Ti, is greater than one. In such an environment, Landau damping is diminished and the waves can survive for longer times. This may be an argument both for or against the waves being real.

5. The low frequency (<0.1 Hz) electric field measurements at times of the observed triggered waves are as expected, which suggests that the instrument functioned nominally at such times. Figure A1 presents four hours of data that illustrate this fact. Panel (a) of this figure gives the power spectrum of Ex which, on careful viewing, is seen to be composed of pulses of energy corresponding to the bursts of the high frequency component of the phase locked wave. Thus, triggered ion-acoustic waves were present through most of the interval. Panels (b) and (c) present the two low frequency components of the electric field and the components of –**v**x**B.** The agreements between the electric field measurements and –**v**x**B** shows that the low frequency electric fields were well-measured. The fields were produced by least-squares fitting the electric field to –**v**x**B**. The two least-squares coefficients produced in this way are the effective antenna length of panel (d) and the angular rotation of the X-Y plane in panel (e) [Mozer et al, 2020a]. The reasonableness of these quantities as well as the excellent agreement between **E** and **–v**x**B** show that the low frequency electric field was well-measured, so there may be less concern about the validity of higher frequency measurements.

6. Because the antennas on the Parker Solar Probe are not much larger than the spacecraft body, it is possible, under certain geometric conditions, that one or more antennas might be in the vehicle wake to produce a spurious wave electric field. In fact, cases of spurious whistler waves have been reported [Malaspina et al, 2022]. To test for this possibility, Figure A2 gives the solar wind speed (panel (c)), the angle of the magnetic field from the Z-direction (panel (d)), the plasma density (panel (e)), and the ion temperature (panel f)). During this four hour interval, the solar wind speed varied by 50%, the angle of the magnetic field relative to the Z-direction varied by 90 degrees, and there were important changes in the plasma density and temperature. None of these variations affected the electric field measurements, which provides evidence that wake or other near-spacecraft effects did not infuence the electric field measurements.

7. Further evidence that the measured fields are physical comes from examination of the four antenna potentials, typical examples of which are presented in Figure A3. The four antenna voltages, filtered from 1-100 Hz, are presented in panels (a), (b), (c), and (d), while the same data, filtered above 100 Hz, are in the bottom four panels. At both the low and high frequency triggered ion acoustic wave frequencies, all four antennas produced good electric potentials with no indication of one or more being perturbed by a wake or any other non-physical effect. Because this behaviour existed during all events, it represents strong evidence that the triggered ion acoustic waves are a real physical phenomenon.

8. On rare occasions a dust strike on the spacecraft turns on or off the triggered ion-acoustic waves. Figure A4 provides examples where this both does and does not happen following large voltage spikes. Panels (A) and (B) of this figure give EX and EY, whose triggered ion-acoustic waves were unaffected by the large voltage pulse that occurred near the center of the plots. By contrast, panels (C) and (D) describe a marginally unstable triggered ion-acoustic wave whose high frequency component was sometimes off and sometimes on until the large voltage spike near the center of the plots produced triggered ion-acoustic waves. This result is surprising because the plasma produced by such a dust impact disappears from the spacecraft vicinity in a fraction of a second. Because the wavelengths of the two triggered waves were orders-of-magnitude larger than the region affected by a dust strike, it is hard to understand this result in either the case of a good triggered wave or an artifact. It remains possible that the voltage spikes induced a form of "ringing" in the detection system, which could then be misinterpreted as ion-acoustic waves. Because observations of dust strikes producing triggered ion-acoustic waves are rare (only a few have been found) it is unlikely that they are the source of the many hours of observed waves on every orbit.

The above analyses suggest that the triggered ion-acoustic waves represent a physical process in the solar wind but they do not rule out an artificial source.

VI REFERENCES

Agapitov O., Drake J. F., Vasko I., Mozer F. S., Artemyev A., Krasnoselskikh V., Angelopoulos V., Wygant J., Reeves G. D., "Nonlinear Electrostatic Steepening of Whistler Waves: The Guiding Factors and Dynamics in Inhomogeneous Systems", Geophysical Research Letters, vol. 45, no. 5, pp. 2168–2176, 2018. doi:10.1002/2017GL076957.

An X., Li, J., Bortnik J., Decyk V., Kletzing C., and Hospodarsky G., "Unified View of Nonlinear Wave Structures Associated with Whistler-Mode Chorus", Physical Review Letters, vol. 122, no. 4, 2019. doi:10.1103/PhysRevLett.122.045101.

Bale, S.D., Goetz, K., Harvey, P.R., Turin, P. Bonnell, J. W., Dudok de Wit, T., Ergun,R.E., MacDowall, R. J., Pulupa, M.; Andre, M., et al, "The Fields Instrument Suite for Solar Probe Plus", SSRv, 204, 49 (2016)

Cattell, C., Breneman, A., Dombeck, J., Hanson, E., Johnson, M., Halekas, J., Bale, S.D., Dudek de Wit, T., Goetz, K., Goodrich, K., Malaspina, D., Pulupa, M., Case, T., Kasper, J.C., Larson, D., Stevens, M., Whittlesey, P., "Parker Solar Probe Evidence for the Absence of Whistlers Close to the Sun to Scatter Strahl and to Regulate Heat Flux,' The Astrophysical Journal Letters, **924,** doi:10.3847/2041-8213/ac4015, (2022)

Davidson, R.C., "Methods in nonlinear plasma theory", eBook ISBN: 9780323153386, Elsevier, (1972)

Fox, N.J., Velli, M.C., Bale, S.D., Decker,R., Driesman, A., Howard, R.A., Kasper, J.C., Kinnison, J., Kusterer, J., Lario, D., et al, "The solar probe mission: humanity's first visit to a star", SSRv, 204, 7 (2016)

Gary S. P. and Omidi N., The ion-ion-acoustic instability, Journal of Plasma Physics, vol. 37, no. 1, pp. 45–61, 1987. doi:10.1017/S0022377800011983.

Hull A. J., Larson, D.E., Wilber, M., Scudder, J.D., Mozer, F.S., Russell, C.T., and Bale, S.D. ., Large-amplitude electrostatic waves associated with magnetic ramp substructure at Earth's bow shock, Geophysical Research Letters, vol. 33, no. 15, doi:10.1029/2005GL025564. (2006)

Kasper, J. C., Abiad, R., Austin, G., Balat-Pichelin, M., Bale, S.D., Belcher, J.W., Berg, P., Bergner, H., Berthomier, M., Bookbinder, J., et al, Solar Wind Electrons Alphas and Protons (SWEAP) Investigation: Design of the Solar Wind and Coronal 171 Plasma Instrument Suite for Solar Probe Plus. Space Sci. Rev. 204, 131–186, DOI 10.1007/s11214-015-0206-3. (2016)

Kelley, M. C. and Mozer, F. S., A technique for making dispersion relation measurements of electrostatic waves, Journal of Geophysical Research, vol. 77, no. 34, pp. 6900–6903. doi:10.1029/JA077i034p06900 (1972).

Kellogg, P.J. A fundamental instability for the solar wind, The Astrophysical Journal, Volume 925, Number 2, (2022)

Kurth, W. S., Gurnett, D. A., and Scarf, F. L., High-resolution spectrograms of ion-acoustic waves in the solar wind, Journal of Geophysical Research, vol. 84, no. A7, pp. 3413–3413. doi:10.1029/JA084iA07p03413 (1979).

Malaspina, D.M., Tigik, S., Vaivads, A., "Evidence that interaction with the Spacecraft Plasma Wake Generates Plasma Waves Clost to the Electron Cyclotron Frequency in the Near-Sun Solar Wind,' The Astrophysical Journal Letters, **936**, doi:10.3847/2041-8213/ac8c8f, (2022)

Mozer, F. S., Agapitov, O. V., Bale, S. D., Bonnell, J. W., Bowen, T. A., & Vasko, I., DC and low-frequency electric field measurements on the Parker Solar Probe. Journal of Geophysical Research: Space Physics, 125, e2020JA027980. https://doi.org/10.1029/2020JA027980, (2020a).

Mozer, F. S., Bonnell, J. W., Bowen, T. A., Schumm, G., and Vasko, I. Y., Large-amplitude, Wideband, Doppler-shifted, Ion-acoustic Waves Observed on the Parker Solar Probe, The Astrophysical Journal, vol. 901, no. 2. doi:10.3847/1538-4357/abafb4 (2020).

Mozer, F.S., Vasko, I.Y., and Verniero, J.L., "Triggered Ion-acoustic Waves in the Solar Wind", The Astrophysical Journal Letters, 919:L2, 2021, https://doi.org/10.3847/2041-8213/ac2259 (2021)

Mozer, F.S., Bale ,S.D., Cattell , C.A., Halekas, J. ,Vasko, I.Y. , Verniero, J.L. , and Kellogg, P.J., "Core Electron Heating by Triggered Ion-acoustic Waves in the Solar Wind", The Astrophysical Journal Letters, 927:L15, 2022a, https://doi.org/10.3847/2041-8213/ac5520, (2021a)

Mozer, F.S., Bale, S.D., Kellogg, P.J., Larson, D.E., Livi, R., and Romeo, O., "An Improved Technique for Measuring Plasma Density to High Frequencies on the Parker Solar Probe", The Astrophysical Journal, 926:220, 2022b, https://doi.org/10.3847/1538-4357/ac4f42, (2022b)

Roytershteyn V. and Delzanno G. L., "Nonlinear coupling of whistler waves to oblique electrostatic turbulence enabled by cold plasma", Physics of Plasmas, vol. 28, no. 4, 2021. doi:10.1063/5.0041838.

Vasko I. Y., Agapitov O., Mozer F. S., Bonnell J. W., Artemyev A. V., Krasnoselskikh V. V., Tong Y., "Electrostatic Steepening of Whistler Waves", Physical Review Letters, vol. 120, no. 19, 2018. doi:10.1103/PhysRevLett.120.195101.

Vasko, I.Y., Mozer, F.S., Bale, S.D., and Artemyev, A.V., "Ion-Acoustic Waves in a Quasi-Perpendicular Earth's Bow Shock", Geophysical Research Letters, vol. 49, no. 11, doi: 10.1029/2022GL098640. (2022)

Whittlesey, P.L., Larson, D.E., Kasper, J.C. Halekas, J., Abatcha, M., Abiad, R., Berthomier, M., Case, A.W., Chen, J., Curtis, D.W., et al, "The Solar Probe ANalyzers—Electrons on the Parker Solar Probe" ,The Astrophysical Journal Supplement Series, 246:74 (14pp), February https://doi.org/10.3847/1538-4365/ab7370 © 2020. (2020)

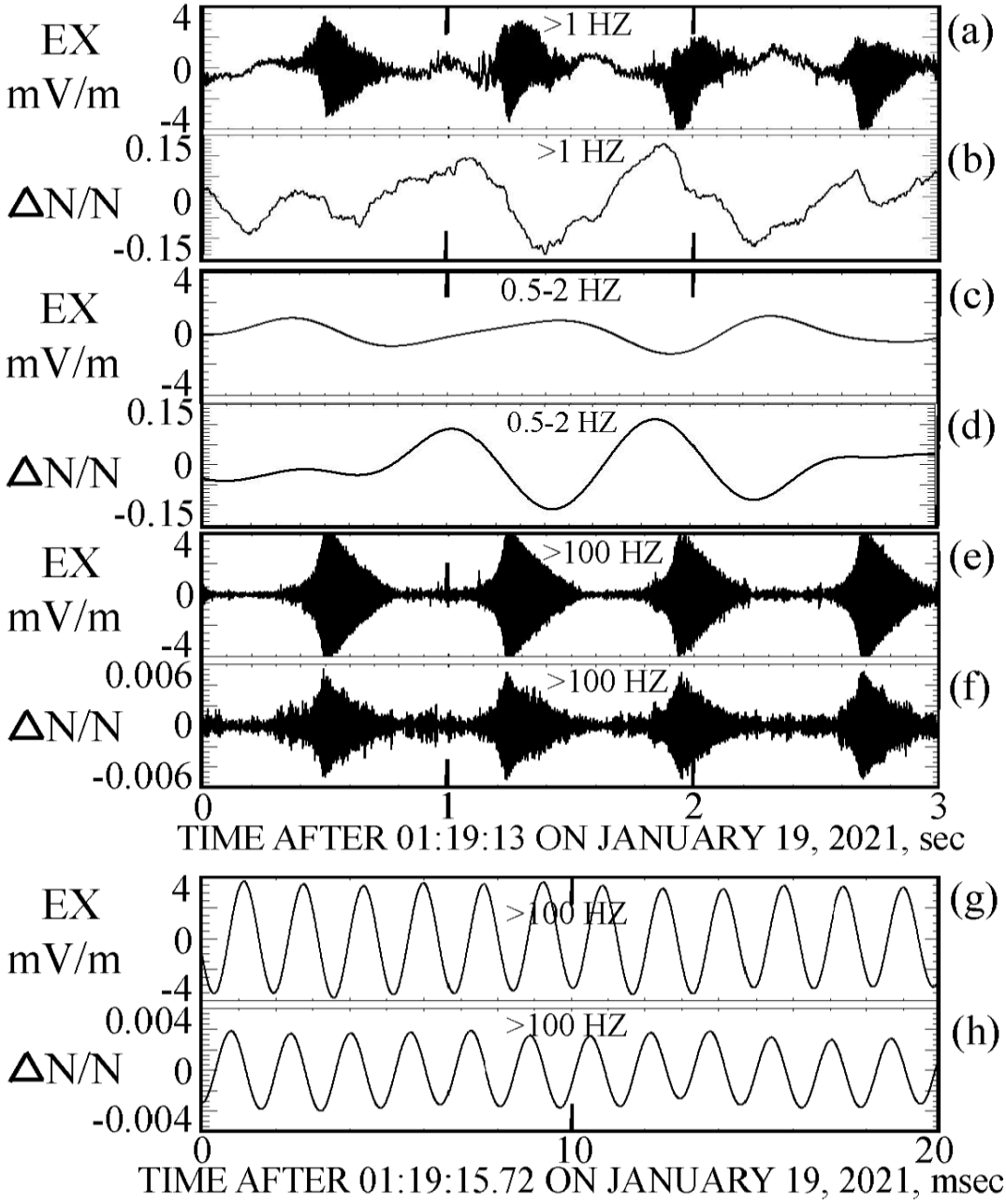

Figure 1. Four pairs of measurements of EX and density fluctuations. The pair (a), (b) are high pass filtered at 1 Hz to display the phase locked low and high frequency signatures of the triggered ion-acoustic wave. Panels (c) and (d) are bandpass filtered at 0.5-2 Hz to display the low frequency components of the wave. The pair (e), (f) are high pass filtered at 100 Hz to show the high frequency component. The pair (g), (h) provide >100 Hz filtered data over a short time interval to illustrate the pure sine wave nature of the high frequency component.

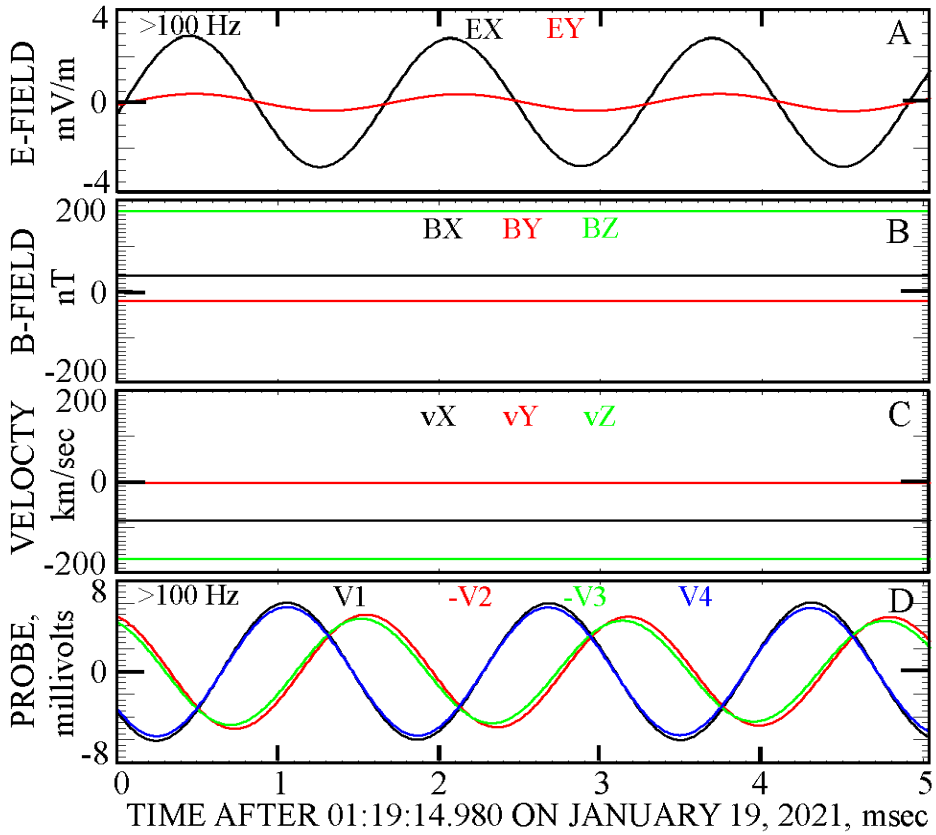

Figure 2. The >100 Hz EX and EY (panel A), the 200 nT magnetic field vectors in the X-Y-Z frame (panel B), the 200 km/sec solar wind velocity (panel C), and the timing of the signals received by the four antennas for the event of Figure 1 (panel D).

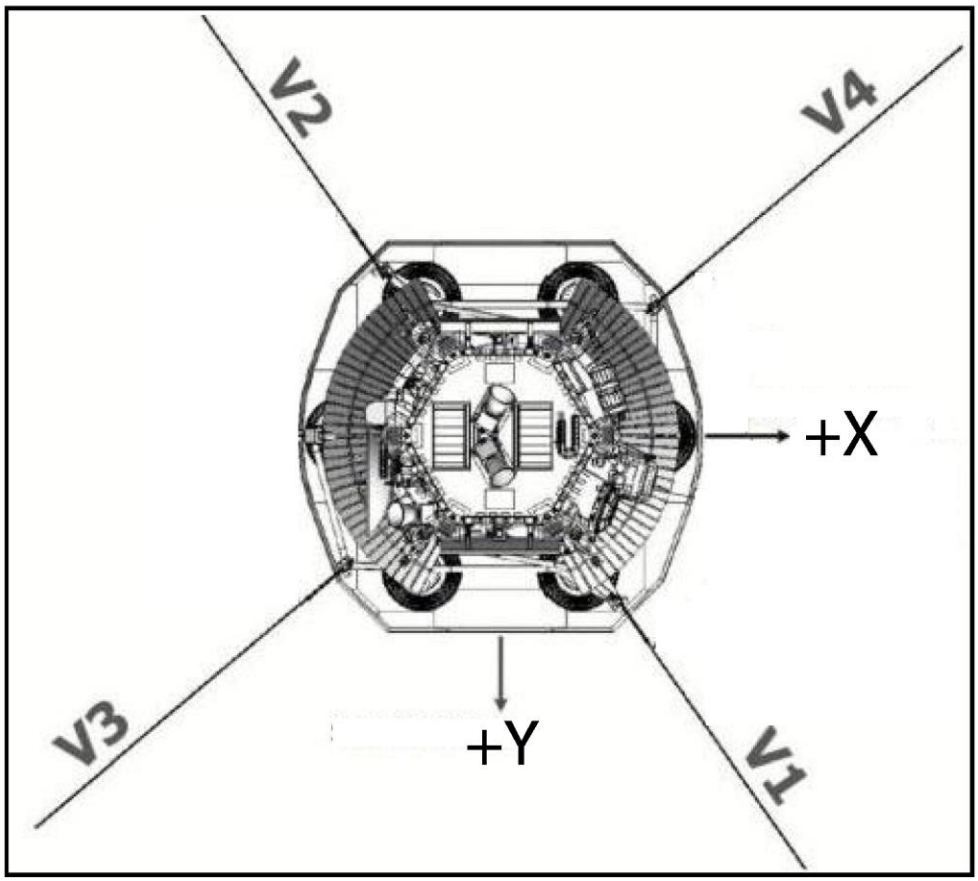

Figure 3. Orientation of the electric field antennas with respect to the X and Y axes.

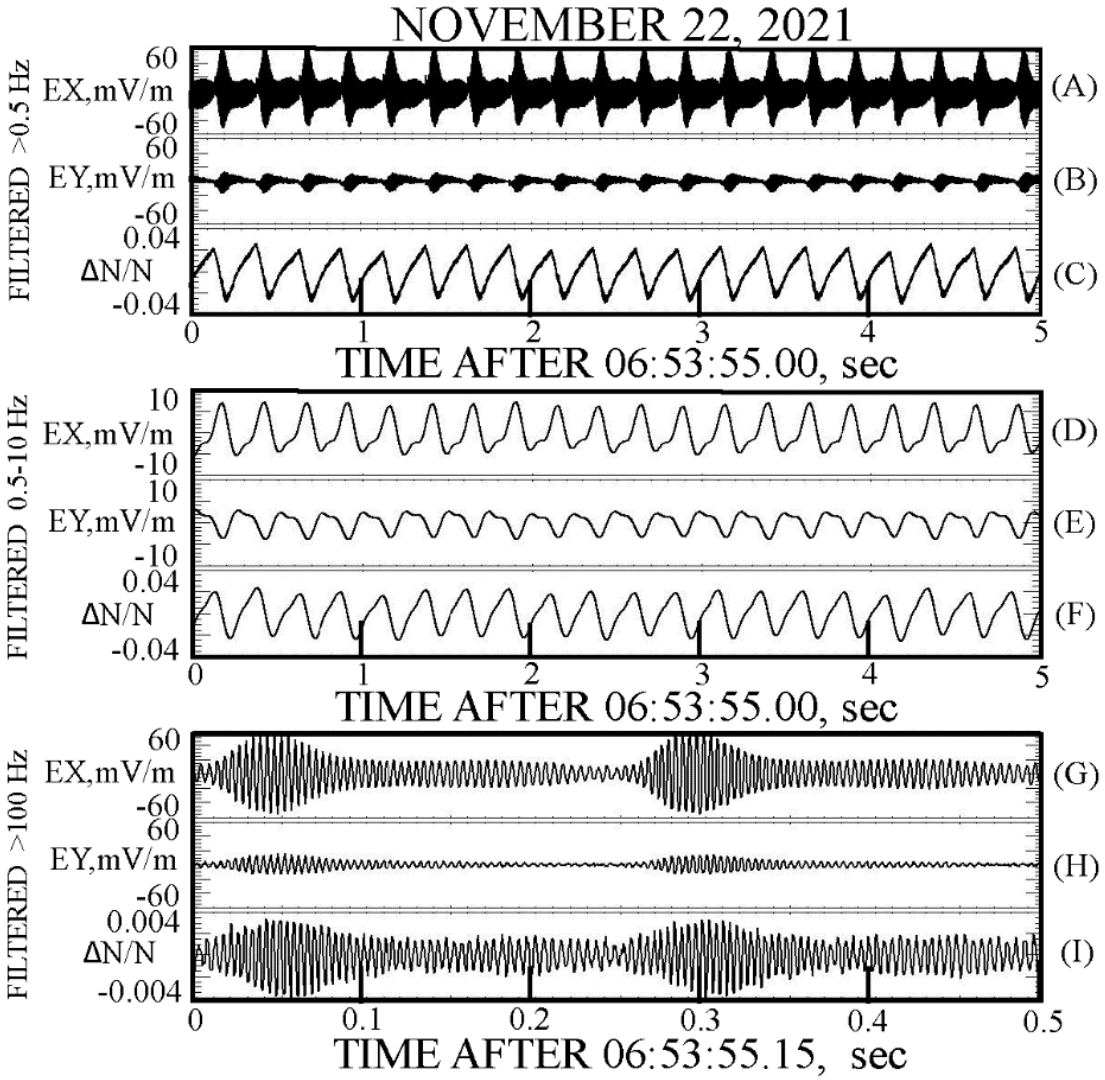

Figure 4. Illustration of a triggered ion-acoustic wave whose high frequency component appeared continuously during the low frequency component, as seen in panels A, B, and C, which present the >0.5 Hz filtered EX. EY, and density fluctuations. Panels D, E, and F give the same quantities that are band pass filtered between 0.5 and 10 Hz in order to more clearly illustrate the low frequency wave components. Panels G, H, and I present 0.5 second segments of the >100 Hz fields and density fluctuations in order to illustrate the pure sine wave nature of the signals.

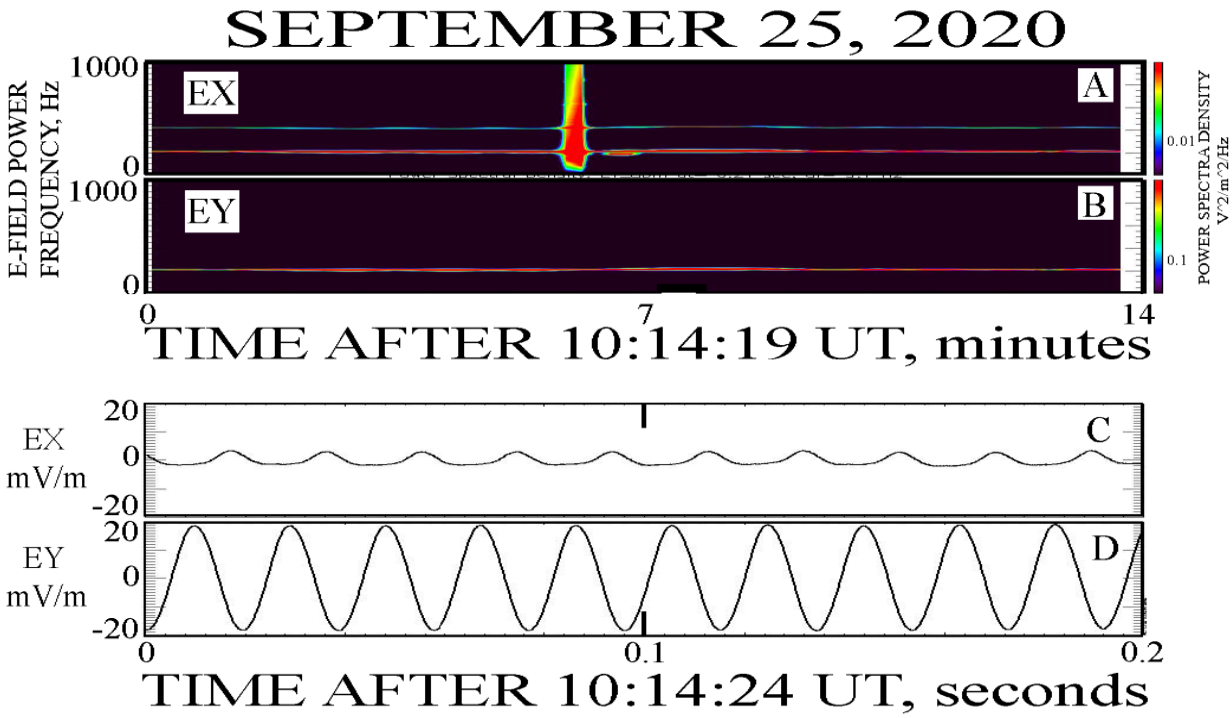

Figure 5. A long duration, pure sine, ion-acoustic wave. Panels 5A and 5B show narrow line spectra. Panels 5C and 5D illustrate short segments of the >100 Hz 14-minute duration waveform, showing that they are nearly pure sine waves. The vertical line near the middle of the event is a dust impact on the spacecraft.

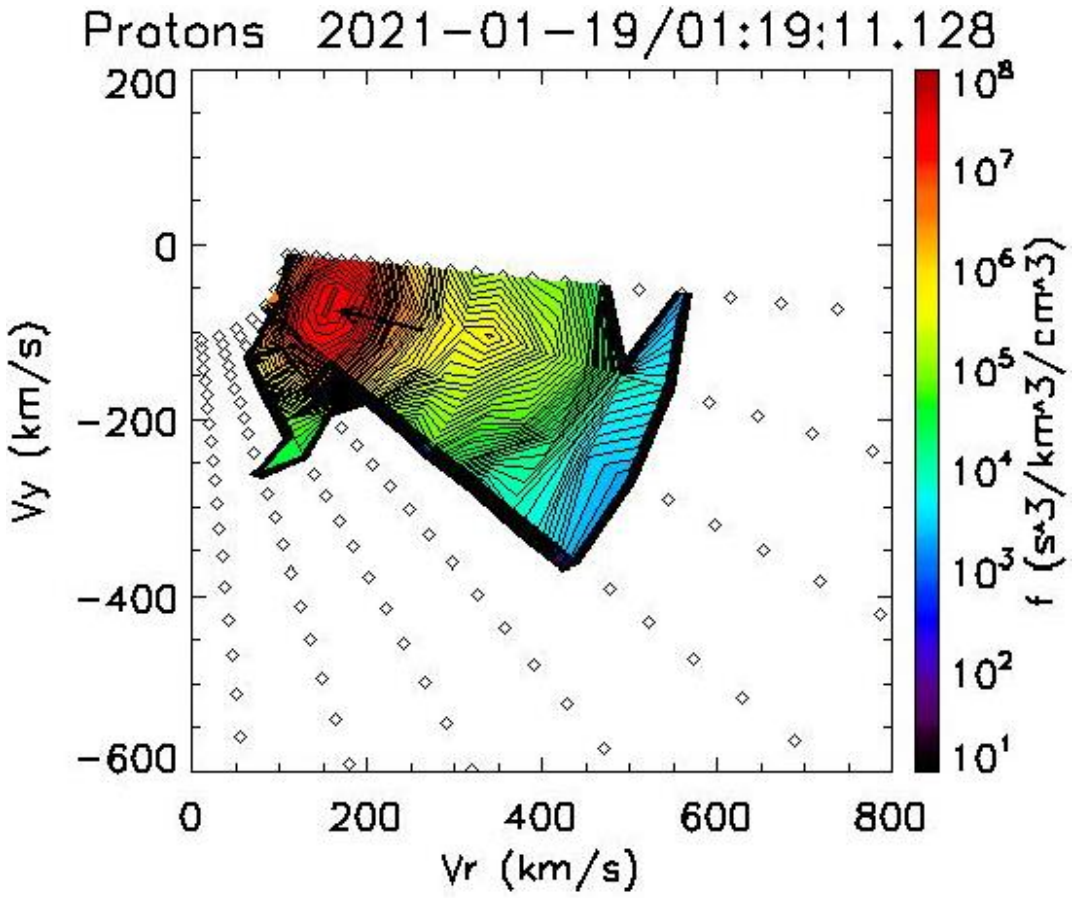

Figure 6. The proton velocity distribution function at the time of interest, showing a beam traveling at ~200 km/sec.

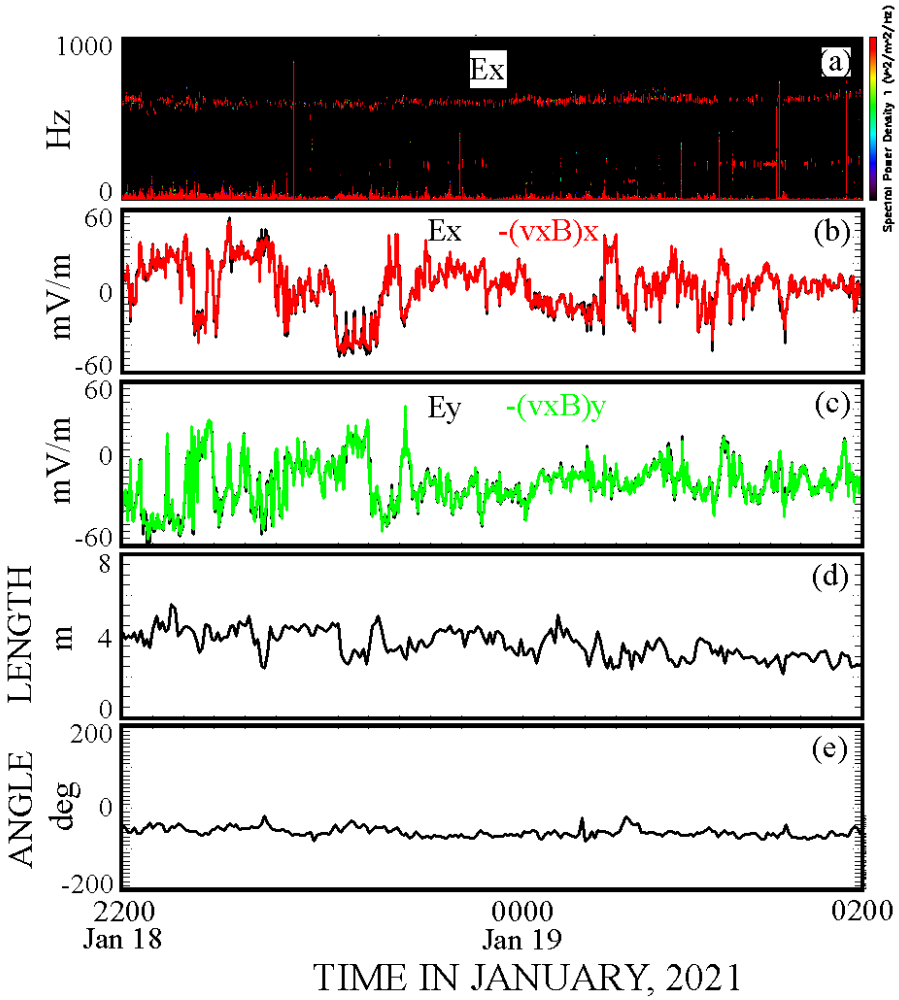

Figure A1. A four hour interval illlustrating the accuracy of the low frequency (<0.1 Hz) electric field measureents. Panel (a) gives the electric field spectrum which, on close examination, consists of a series of red dots showing that the 600 Hz pure sine wave occurred in triggered bursts through the interval. Panel (b) gives the dc and low frequency X-component of the electric field and the X-component of –vxB. Panel (c) provides the same data for the Y-compnents. The agreement between **E** and –**v**x**B** shows that the instrument functioned normally during this interval. The electric field is obtained from a least-squares fit and the two least-squares coefficients are shown in panels (d) and (e) [Mozer et al, 2020a].

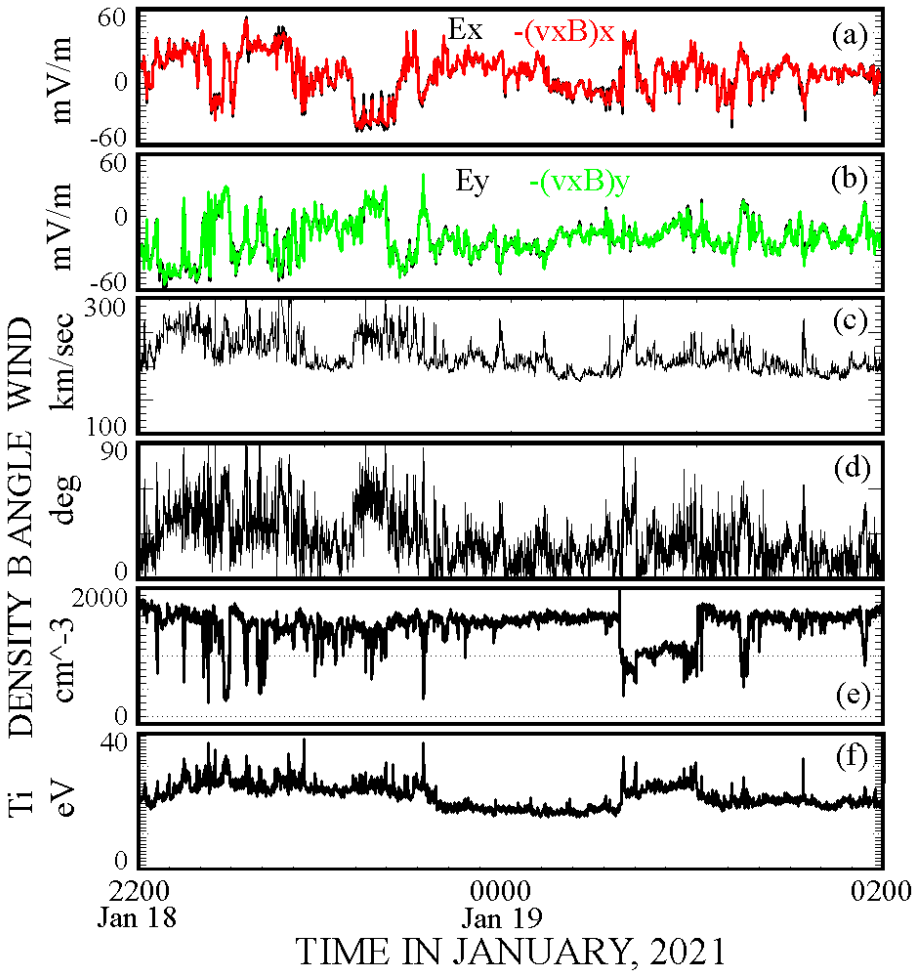

Figure A2. The solar wind speed (c), the angle of the magnetic field with respect to the Z-direction (d), the plasma density (e), and the ion temperature during the four hour interval of interest. The magnetic field rotated through as much as 90 degrees while the solar wind speed varied by 50%, all of which occurred during good electric field measurements. This result suggests that the electric field data were not perturbed by wake or similar effects.

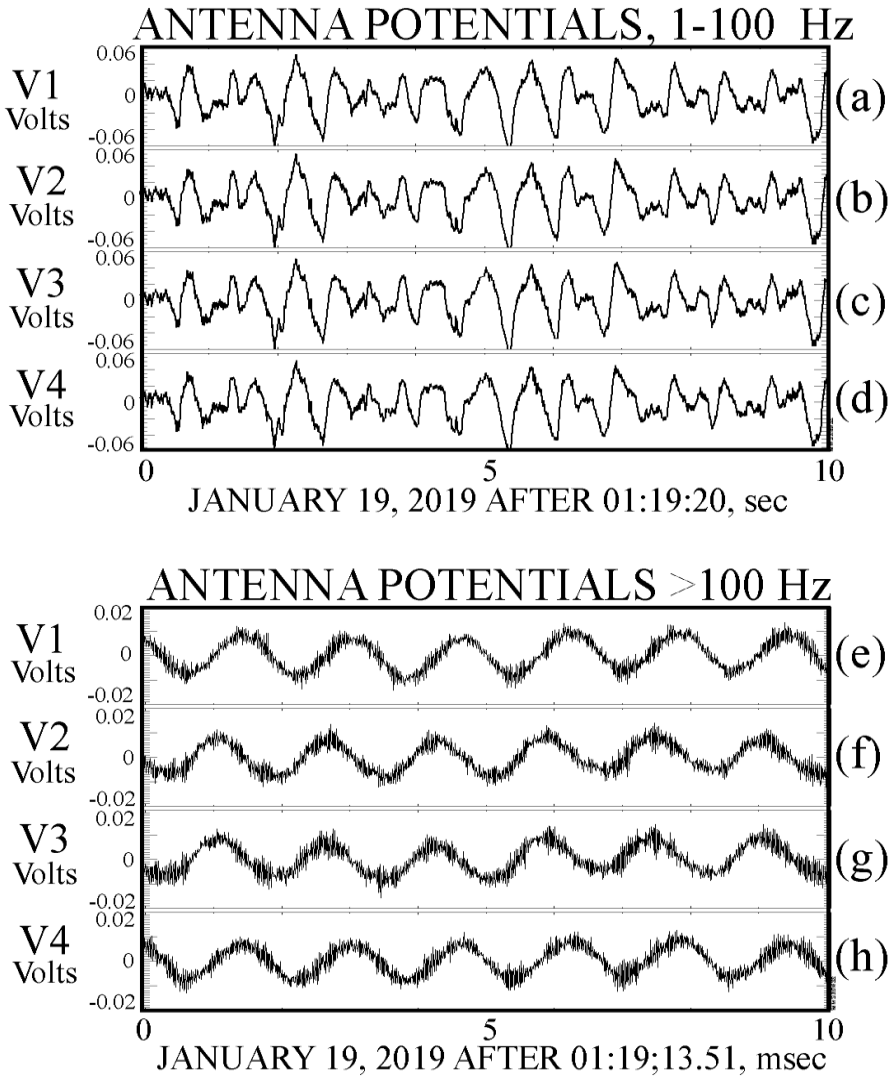

Figure A3. Typical four antenna potentials at the two frequencies of the triggered ion acoustic waves. In both cases, all of the antennas operated normally with no indication of one or more of them being affected by a wake or other non-physical process. This provides strong evidence that the observed waves were physical and not an artifact resulting from a wake or a detector malfunction.

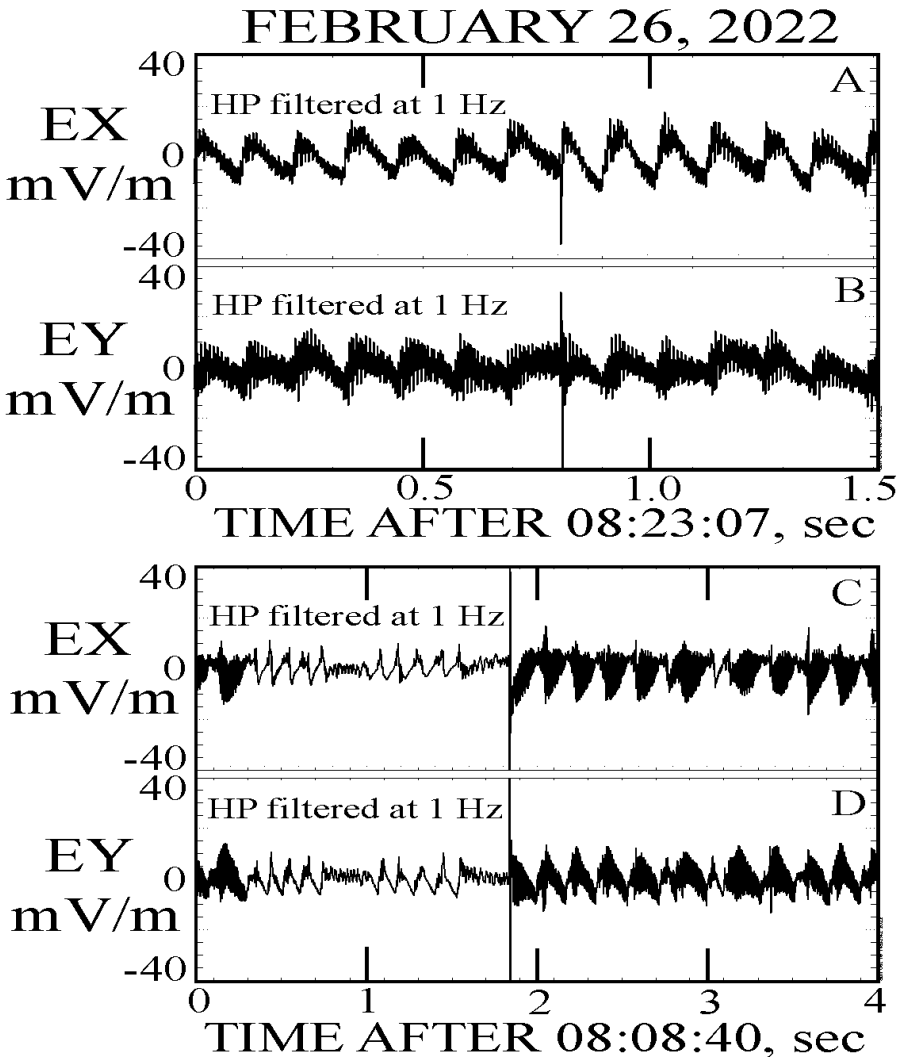

Figure A4. Two examples of triggered ion-acoustic waves in the presence of large amplitude voltage spikes. Panels (A) and (B) give EX and EY, whose triggered ion-acoustic waves were unaffected by the large voltage pulse that occurred near the center of the plots. By contrast, panels (C) and (D) describe a marginally unstable triggered ion-acoustic wave whose high frequency component was sometimes off and sometimes on until the large voltage spike near the center of the plots drove the plasma unstable to the generation of the high frequency component and full, typical, triggered ion-acoustic waves resulted.